Analysis of Stiffness in the Immersed Boundary Method and Implications for Time-stepping Schemes

[submitted to *J. Comput. Phys.*, June 1998]

John M. Stockie
Department of Mathematics and Statistics
Simon Fraser University
Burnaby, British Columbia, Canada V5A 1S6
jms@cs.sfu.ca

Brian R. Wetton
Department of Mathematics
University of British Columbia
Vancouver, British Columbia, Canada V6T 1Z2
wetton@math.ubc.ca

Subject classification: 65M06, 65M12, 73K70, 35B30
Key words: immersed boundary method, linear stability, time-stepping schemes

Abstract

The immersed boundary method is known to exhibit a high degree of numerical stiffness, which is associated with the interaction of immersed elastic fibres with the surrounding fluid. We perform a linear analysis of the underlying equations of motion for immersed fibres, and identify a discrete set of *fibre modes* which are associated solely with the presence of the fibre. These results are a generalisation of those in a previous paper (*SIAM J. Appl. Math.*, 55(6):1577-1591, 1995) by including the effect of spreading the singular fibre force over a finite "smoothing radius," which corresponds to the approximate delta function used in the immersed boundary method. We investigate the stability of the fibre modes, their stiffness and dependence on the problem parameters, and the effect that smoothing has on the solution.

The analytical results are then extended to include the effects of time discretisation, and conclusions are drawn about the time step restrictions on various explicit time-stepping schemes, as well as the convergence rates for an iterative semi-implicit method. Comparisons are drawn with computations, and we show how the results can be applied to help in choosing alternate time-stepping schemes that are specially-tailored to handle the stiffness in immersed fibres. In particular, we present numerical results that show how fully explicit Runge-Kutta schemes perform comparably with the best of semi-implicit schemes currently in use.

1 Introduction

Some of the most challenging problems in scientific computation involve the interaction of a viscous fluid with complex, moving boundaries. One approach that has proven particularly effective in handling a variety of such problems is the *"Immersed Boundary Method,"* which was originally developed by Peskin [16] to compute the flow of blood in a two-dimensional model of the heart. The method is a mixed Eulerian-Lagrangian scheme, in which the equations describing the fluid motion are discretised on a fixed, Cartesian mesh, while the immersed boundary is tracked at a set of points that move relative to the underlying fluid grid. The coupling between the fluid and fibre is accomplished using smoothed delta functions, which serve to interpolate quantities between the two grids. The method has since been extended to three-dimensional simulations of flow in the heart and arteries [21, 17] and a diverse collection of other problems, including swimming motions of marine worms [6], particle suspensions [8], and wood pulp fibre dynamics [23], to name a few. Furthermore, the idea of using smoothed delta functions to approximate singular forces generated on internal boundaries is a technique that has recently been applied in concert with a variety of other numerical methods including particle-in-cell [10], finite element [25, 27], and level set methods [3].

Considering the widespread use of immersed boundaries as a modeling and computational tool, very little analysis has been performed on either the underlying model equations or the numerical method. Exact solutions have been derived for simplifications of the immersed boundary problem, specialised for fluid flow in the inner ear [12] and particle suspensions [7]. Beyer and LeVeque [2] analysed a one-dimensional version of the immersed boundary method, and showed that it is limited to first order spatial accuracy by the particular delta function approximation which is used most commonly in practice — this limitation on accuracy has also been confirmed in higher dimensions by numerical tests [11]. In addition, computations indicate that the problem suffers from a high level of numerical stiffness, and considerable effort has gone into developing semi-implicit variations of the method that aim to alleviate the severe time step restrictions by coupling the immersed fibre implicitly with the fluid [26, 13]. However, these attempts have met with limited success, and the majority of computations are still performed using an explicit treatment of the immersed fibres.

Our purpose in this paper is two-fold: first, to examine the stability and stiffness characteristics of incompressible, viscous fluid flows containing moving, elastic fibres; and second, to use these results as a basis for evaluating the efficiency of various explicit and semi-implicit time-stepping schemes for the immersed boundary method. This work is based on an earlier paper [24] that employed a linear stability analysis to identify solution modes arising solely from the presence of an immersed fibre. The severe stiffness observed in computations was traced to the presence of these "fibre modes" in the solution, and is attributed to a combination of small viscosity and large fibre force. Hence, fluid flows with immersed fibres experience something very unlike the usual *Reynolds number limitation* encountered in flows without a fibre. While the previous paper was able to pinpoint the source of the stiffness and its dependence on the problem parameters, it also predicted a time step restriction much smaller than is actually encountered in practice.

In the current paper, we will address this discrepancy by including the effects of smoothing through delta function approximation, and thereby hope to gain a better quantitative measure of the stiffness inherent in fibre modes. We begin in Section 2 with a statement of the equations governing the motion of an isolated fibre immersed in a two-dimensional Stokes flow, and then briefly outline the immersed boundary method. The linear analysis of the immersed fibre problem with a smoothed forcing term is performed in Section 3, which yields a dispersion relation for the fibre modes. The behaviour of these modes is compared to computed solutions and to our earlier work on the analytical solution for the exact delta function problem. Section 4 extends the linear analysis to the time-discrete problem, and uses stability diagrams to investigate the time step restrictions on schemes that are explicit in the fibre force. We also explore a particular semi-implicit discretisation, in which the scheme can be formulated as an iteration on the fibre position, and verify the predicted convergence rates in numerical experiments. Through comparisons of the various time-stepping schemes, we show that a fully explicit, fourth order Runge-Kutta method can be competitive with the implicit schemes that are currently in use.

2 Immersed fibres

For the remainder of this work, we will consider an isolated fibre, Γ, immersed within a rectangular domain Ω that is filled with a viscous, incompressible fluid (refer to Fig. 1). We single out a lone fibre for reasons of mathematical convenience, a simplification which seems reasonable when one considers that even the most complex immersed surfaces in three dimensions, such as the 3D heart model in [17], are constructed of interwoven networks of such fibres. In the immersed boundary model, the fibre is assumed to be massless and

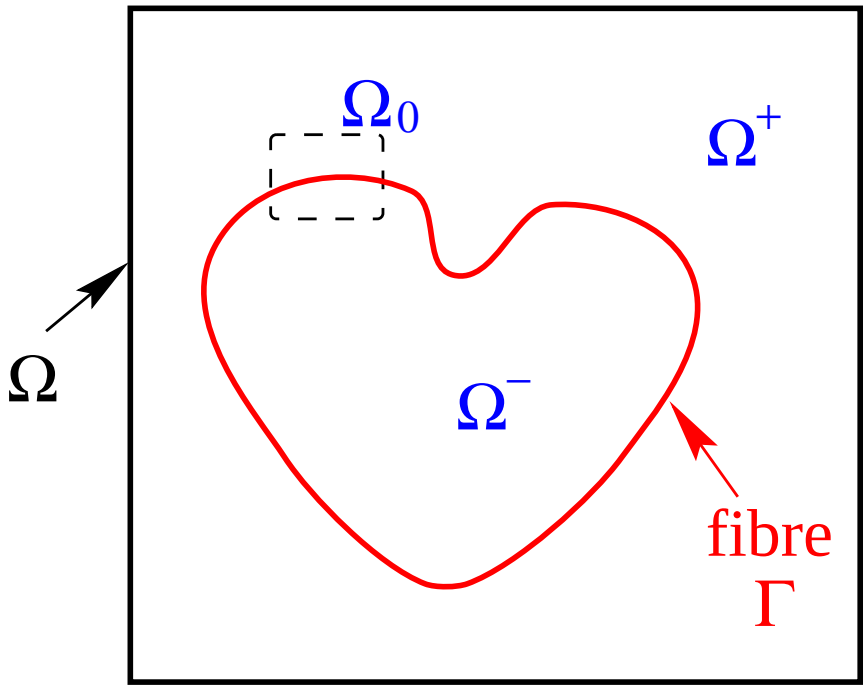

Figure 1: The two-dimensional model: a fluid domain, Ω, which is divided into two parts, Ω^+ and Ω^-, by an immersed fibre Γ.

neutrally-buoyant, so that the fluid and fibre can be treated as a composite, viscoelastic material, described by a single velocity field. This is the major advantage of the model, since it allows the fluid and fibre to be described by the same set of equations, which is described next.

2.1 Mathematical formulation

Consider a square fluid domain, $\Omega = [0,1] \times [0,1]$, with periodic boundary conditions in both the x– and y–directions. The motion of the fluid-fibre composite is governed by Stokes' equations

$$\rho \frac{\partial \boldsymbol{u}}{\partial t} = \mu \Delta \boldsymbol{u} - \nabla p + \boldsymbol{F}, \tag{1}$$

$$\nabla \cdot \boldsymbol{u} = 0, \tag{2}$$

where $\boldsymbol{u}(\boldsymbol{x},t) = (u(\boldsymbol{x},t), v(\boldsymbol{x},t))$ is the fluid velocity, $p(\boldsymbol{x},t)$ the pressure, $\boldsymbol{F}(\boldsymbol{x},t)$ is the fluid body force, and ρ and μ are the (constant) fluid density and viscosity.

Our reason for considering Stokes' equations (and ignoring the effects of convection) is that the serious numerical stability problems encountered in computations are well-known to arise from the stiffness in the immersed boundary. While high Reynolds number flows do require a finer mesh to resolve the boundary

layer effects around complex elastic structures, and thereby naturally require a smaller time step, there is no inherent Reynolds number limit on the immersed boundary method. The method is not tied to a specific fluid solver, and even when using alternate solvers specially-tailored to handle convection-dominated flows, the stiffness in the immersed fibres is still the major consideration [14, 20].

The position of the fibre is given by $\boldsymbol{x} = \boldsymbol{X}(s,t)$, where s is a parameterisation of Γ in some reference configuration. Since the fibre is constrained to move at the same velocity as neighbouring fluid particles, we can write

$$\frac{\partial \boldsymbol{X}}{\partial t} = \boldsymbol{u}(\boldsymbol{X}(s,t),t). \tag{3}$$

One more element is needed to close the system: namely, an expression for the force $\boldsymbol{F}$ to couple the motion of the fluid and fibre. Gravitational effects are assumed to be negligible since the fibre is neutrally buoyant, and so the external force $\boldsymbol{F}$ arises solely from the action of the elastic fibre. Let $T(s,t)$ be the tension force in the fibre and assume that T is a function of the fibre strain:

$$T = T\left(\left|\frac{\partial \boldsymbol{X}}{\partial s}\right|\right). \tag{4}$$

It can be shown under further assumptions [17] that the local force density per unit length is given by the expression

$$\boldsymbol{f}(s,t) = \frac{\partial}{\partial s}(T\boldsymbol{\tau}), \tag{5}$$

where τ is the unit tangent vector to the fibre. For example, if the tension depends linearly on the strain as $T = \sigma\,|\partial \boldsymbol{X}/\partial s|$, then Eq. (5) reduces to

$$\boldsymbol{f} = \sigma\,\frac{\partial^2 \boldsymbol{X}}{\partial s^2}. \tag{6}$$

Taking this form of the force is analogous to linking successive fibre points by linear springs with spring constant σ and zero resting length — we will see a similar forcing function appearing in the linear stability analysis in Section 3.

Since the force is zero everywhere except on the fibre, the fluid body force $\boldsymbol{F}$ can be regarded as a distribution and written compactly as the convolution of the fibre force density with a delta function:

$$\boldsymbol{F}(\boldsymbol{x},t) = \int_\Gamma \boldsymbol{f}(s,t)\cdot\delta(\boldsymbol{x}-\boldsymbol{X}(s,t))\,ds. \tag{7}$$

The two-dimensional delta function $\delta(\boldsymbol{x}) = \delta(x)\cdot\delta(y)$ is the product of two Dirac delta functions. Finally, we rewrite the right hand side of the fibre evolution equation (3) in the form of a convolution of the velocity with a delta function

$$\frac{\partial \boldsymbol{X}}{\partial t} = \int_\Omega \boldsymbol{u}(\boldsymbol{x}(s,t),t)\cdot\delta(\boldsymbol{x}-\boldsymbol{X}(s,t))\,d\boldsymbol{x}, \tag{8}$$

thereby introducing a symmetry between Eqs. (7) and (8). This will prove to be very useful in Section 2.2 from the standpoint of constructing a numerical scheme. Eqs. (1), (2) and (8), along with the definition of the fibre force in (4), (5) and (7), form a coupled system of integro-differential equations for the motion of the fluid and fibre.

It is important to mention that there is another equivalent formulation of the problem, in which the singular delta function terms are supplanted with jump conditions, relating values of the fluid stress on either side of the fibre. This "jump formulation" was used as the basis of our analysis in [24], but is inappropriate for the current work, where our aim is to determine the effect of replacing the delta function with a smooth approximation.

2.2 Immersed boundary method

We will state the immersed boundary method in a form very similar to that originally proposed by Peskin [16], and which is still currently in use. This scheme is explicit in the fibre force, and any discussion of details related to semi-implicit discretisations will be postponed until Section 4 when they are needed.

The fluid domain is divided into a fixed, $N \times N$ grid of points denoted $\vec{x}_{i,j} = (x_i, y_j) = (ih, jh)$, with spacing $h = \frac{1}{N}$ in both directions. The domain is doubly-periodic so that the points x_0 and x_N are identified with each other, and similarly with y_0 and y_N. The fibre position is a Lagrangian quantity which is discretised at a set of N_b moving points, with the parameter $s \in [0, 1]$ taken at discrete locations $s_\ell = \ell \cdot h_b$, where $h_b = \frac{1}{N_b}$. Both fluid and fibre unknowns are sampled at equally-spaced time intervals $t_n = n \cdot k$, where k is the time step. Figure 2 shows a typical fluid-fibre grid, where the respective grid points need not necessarily coincide. The discrete approximation for the fluid velocity is written as $\vec{u}^n_{i,j} \approx \boldsymbol{u}(x_i, y_j, t_n)$ at fluid grid

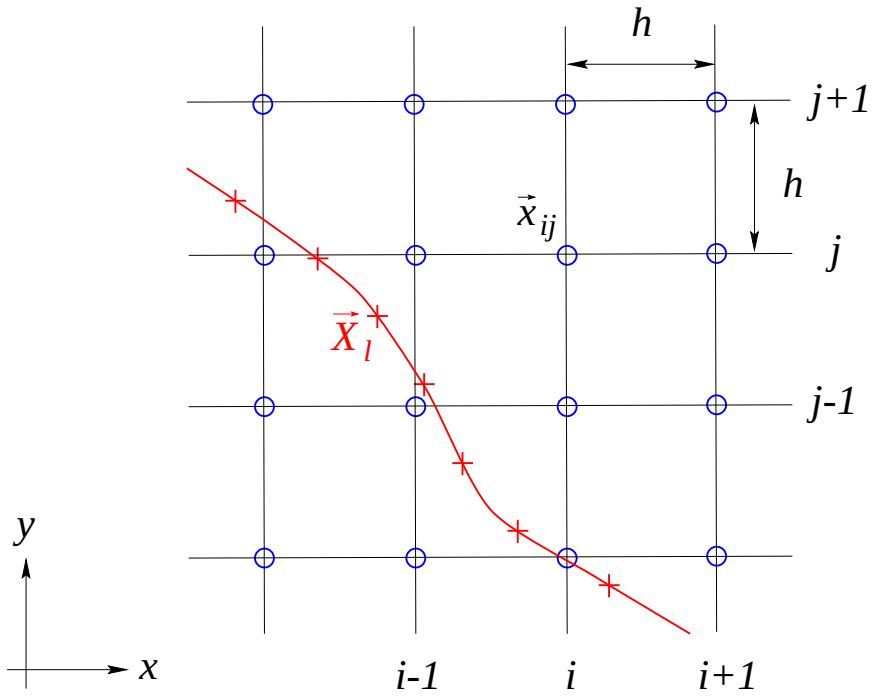

Figure 2: The relationship between fluid (∘) and fibre (+) grid points.

points $i, j = 0, 1, \ldots, N-1$ and $n = 0, 1, \ldots$ (with analogous expressions for pressure and force). Similarly, the fibre quantities are written using the notation $\vec{X}^n_\ell \approx \boldsymbol{X}(s_\ell, t_n)$, where $\ell = 0, 1, \ldots, N_b - 1$.

The delta functions appearing in (7) and (8) are replaced by an approximation $\delta_{2h}(\boldsymbol{x})$, which is the product of two one-dimensional discrete delta functions

$$\delta_{2h}(x_i, y_j) = d_{2h}(x_i) \cdot d_{2h}(y_j).$$

The choice of d_{2h} most commonly used in immersed boundary computations is

$$d_{2h}(r) = \begin{cases} \frac{1}{4h}\left(1 + \cos\frac{\pi r}{2h}\right) & \text{if } |r| < 2h, \\ 0 & \text{if } |r| \geq 2h, \end{cases} \tag{9}$$

although other choices are possible (refer to [22] for alternate forms of d_{2h}). It will become clear in the algorithm to follow that $\delta_{2h}(\boldsymbol{x})$ acts to interpolate quantities between the fluid and fibre grid points.

When writing the scheme, we will make use of the following notation for finite difference operators on the fluid grid. First and second derivatives are approximated using the second order centered difference formulas

$$D_x \phi_{i,j} = \frac{\phi_{i+1,j} - \phi_{i-1,j}}{2h} \qquad \text{and} \qquad D_{xx} \phi_{i,j} = \frac{\phi_{i+1,j} - 2\phi_{i,j} + \phi_{i-1,j}}{h^2}$$

respectively, with similar approximations for first and second y–derivatives, D_y and D_{yy}. The discrete gradient and Laplacian operators are then given by

$$\nabla_h \phi_{i,j} = (D_x,\, D_y)\, \phi_{i,j} \qquad \text{and} \qquad \Delta_h \phi_{i,j} = (D_{xx} + D_{yy})\, \phi_{i,j}\,.$$

A similar definition is used for the second derivative of fibre quantities, $D_{ss}\psi_\ell$.

We are now in a position to state the algorithm, which is a discrete version of Eqs. (1), (2), (6) and (8). Assuming that the velocity $\vec{u}^n_{i,j}$ and fibre position $\vec{X}^n_{i,j}$ are known at time t_{n-1}, the procedure for updating these values to time t_n is as follows:

STEP 1: Compute the fibre force density

$$\vec{f}^n_\ell = \sigma D_{ss} \vec{X}^{n-1}_\ell, \tag{10a}$$

where we have assumed, for simplicity, that the force is a linear function such as that in Eq. (6).

STEP 2: Distribute the fibre force to fluid grid points

$$\vec{F}^n_{i,j} = \sum_{\ell=0}^{N_b-1} \vec{f}^n_\ell \cdot \delta_{2h}(\vec{x}_{i,j} - \vec{X}^{n-1}_{i,j}) \cdot h_b. \tag{10b}$$

STEP 3: Solve the discrete Stokes problem

$$\rho \left(\frac{\vec{u}^n_{i,j} - \vec{u}^{n-1}_{i,j}}{k} \right) = \mu \Delta_h \vec{u}^n_{i,j} - \nabla_h p^n_{i,j} + \vec{F}^n_{i,j}, \tag{10c}$$

$$\nabla_h \cdot \vec{u}^n_{i,j} = 0, \tag{10d}$$

which is a simultaneous system of equations for the velocity $\vec{u}^n_{i,j}$ and pressure $p^n_{i,j}$ at time level n. Because the fluid grid is rectangular and equally-spaced and the boundary conditions are periodic, this system can be solved very efficiently using a Fast Fourier Transform (see [15] for details).

This approach to solving the fluid equations differs from the *Alternating Direction Implicit* (or ADI) scheme that has been used almost exclusively in immersed boundary computations to this point in time [16]. We have chosen to use the coupled Stokes solver instead because it is a much more natural framework for solving Stokes' equations (and there is no need for the ADI technique when the convection terms are dropped). Furthermore, recent immersed boundary computations [15] have begun to use this same technique, treating the convection terms explicitly instead of in the ADI step. Although we are only concerned with Stokes' equations at the moment, it is worthwhile mentioning that it is possible in practice to discretise the convection terms explicitly, because the time step required for stability of the fibre forcing terms is much smaller than any limitation arising from convection.

STEP 4: Evolve the fibre at the new local fluid velocity

$$\frac{\vec{X}^n_\ell - \vec{X}^{n-1}_\ell}{k} = \sum_{i,j=0}^{N-1} \vec{u}^n_{i,j} \cdot \delta_{2h}(\vec{x}_{i,j} - \vec{X}^{n-1}_\ell) \cdot h^2. \tag{10e}$$

STEP 5: Increment n and return to STEP 1.

Since this algorithm applies an implicit (Backward Euler) discretisation to diffusion terms, and a Forward Euler step for the fibre force and position, we will refer to it as the *"Forward Euler/Backward Euler"* or *FE/BE* method. This designation will also serve to distinguish it from other semi-implicit time-stepping schemes that will be introduced later in Section 4.

3 Linear stability analysis

As mentioned in the Introduction, a great deal of effort has gone into applying the immersed boundary method to various physical problems and improving its efficiency. However, comparatively little work has been done on analysing the behaviour of solutions to the underlying equations of motion. LeVeque and others [12] applied a Fourier transform technique to find an explicit solution to a two–dimensional immersed boundary model of wave propagation in the basilar membrane, which is suspended in the fluid–filled cavity of the inner ear. They used a variation of the immersed fibre equations that was simplified in two ways: stretching of the fibre in the tangential direction is ignored; and the pressure jump is taken to have a special functional form, justified by the physics of the problem. Fogelson [7] has also applied a similar technique to determining the stability of the elastic links between platelets in a model of blood clotting, and more recently, Cortez & Varela [5] performed a non-linear analysis of an immersed elastic fibre in the absence of viscosity.

In this section we will use an approach akin to that in [12, 7] to perform a *linear modal analysis* of the immersed fibre problem in a more general form. It is not possible to solve the full problem explicitly, but we are able to obtain useful information about the stability and conditioning of fluid flows containing immersed fibres, which relates to the stiffness observed in immersed boundary computations.

3.1 Linearisation and smoothing

Consider a portion of the fluid domain, labeled Ω_0 in Figure 1, on which the immersed fibre is approximately flat. Suppose that the fibre is at equilibrium along the horizontal line $y = 0$, and that the current fibre position is a small perturbation from this rest state. For the purpose of isolating the influence of the fibre on the flow, we extend the boundaries of Ω_0 to infinity in the y–direction. We can justify this "stretching" of the fluid domain as follows:

a) The important dynamics that distinguish fluids with immersed fibres from those without should occur in the region near the fibre.

b) In the absence of immersed fibres, there are no non-trivial discrete modes of Stokes' equations on a domain of infinite extent, and so we expect to be able to identify modes associated solely with the fibre by extending the boundaries to infinity.

c) The solution modes that we are most concerned with (that is, which have the most effect on stability) are those with the largest wavenumber, and these are precisely the modes that are least affected by the presence or absence of boundaries.

A common functional form of the fibre tension used in immersed boundary computations [26] is $T = T(|\partial \boldsymbol{X}/\partial s| - 1)$ with $T(0) = 0$, corresponding to a fibre which is slack in the reference configuration $|\partial \boldsymbol{X}/\partial s| = 1$. In practice, however, the fibre is usually under stress. Hence, we choose an equilibrium state defined by $|\partial \boldsymbol{X}/\partial s| = \theta \geq 1$, around which the solution is linearised by supposing a perturbation of the form

$$\boldsymbol{X}(s,t) = (\theta s + \xi(s,t),\, \eta(s,t))\,. \tag{11}$$

We also make the linearity assumptions that ξ, η, $\boldsymbol{u}$ and their derivatives are small, at least for some finite time.

We next incorporate the effect of smoothing the delta function which is integral to the immersed boundary method. To this end, we introduce a strip of width ϵ on either side of the fibre (called the *smoothing region*), where ϵ represents the radius of support of the approximate delta function. The fluid domain, Ω_0, is now divided into three subregions, $\Omega_0^{\pm}$ and Ω_0^{ϵ}, as pictured in Figure 3. The smoothed delta function, which we will write as $d_\epsilon(x)$, is the cosine function introduced earlier in Eq. (9), except that we change notation by replacing h with $\epsilon/2$ (corresponding to the smoothing radius $\epsilon = 2h$ used in the immersed boundary method).

Stokes' equations now read

$$\rho\frac{\partial \boldsymbol{u}}{\partial t} = \mu\Delta\boldsymbol{u} - \nabla p + \int_\Gamma \boldsymbol{f}(s,t)\cdot\delta_\epsilon(\boldsymbol{x}-\boldsymbol{X}(s,t))\,ds, \tag{12}$$

$$\nabla\cdot\boldsymbol{u} = 0, \tag{13}$$

where the integral force term has support only on the smoothing region Ω_0^ϵ, and is equal to zero on $\Omega_0^\pm$. The linearisation of the fibre force expressed by Eqs. (4) and (5) follows that of [24], and so we will simply state the result, that

$$\boldsymbol{f}(s,t) \approx \left(\sigma_t\frac{\partial^2\xi}{\partial s^2},\ \sigma_n\frac{\partial^2\eta}{\partial s^2}\right), \tag{14}$$

where the normal and tangential force coefficients are given by $\sigma_n := T(\theta)/\theta$ and $\sigma_t := T'(\theta)$. Finally, the fibre evolution equation can be written as an integral solely over the smoothing region:

$$\frac{\partial \boldsymbol{X}}{\partial t} = \int_{\Omega_0^\epsilon} \boldsymbol{u}(\boldsymbol{x},t)\cdot\delta_\epsilon(\boldsymbol{x}-\boldsymbol{X}(s,t))\,d\boldsymbol{x}. \tag{15}$$

The remainder of Section 3 is devoted to solving the linearised equations of motion and using the behaviour of the resulting solution modes to answer the following questions:

- *Does the smoothed problem also give rise to a discrete set of "fibre modes"?*
- *Are these fibre modes stable, and how stiff are they?*
- *Does the smoothed analysis lead to any predictions about the behaviour of the numerical solution?*

3.2 Derivation of the dispersion relation

In order to isolate the solution modes that are periodic oscillations in x, we look for separable solutions of Eqs. (12)–(15) that have the form of Fourier modes

$$\left\{\begin{array}{c} u \\ v \\ p \end{array}\right\} = e^{\lambda t + \hat{\imath}\alpha x}\left\{\begin{array}{c} \widehat{u}(y) \\ \widehat{v}(y) \\ \widehat{p}(y) \end{array}\right\} \qquad \text{and} \qquad \left\{\begin{array}{c} \xi \\ \eta \end{array}\right\} = e^{\lambda t + \hat{\imath}\alpha s}\left\{\begin{array}{c} \widehat{\xi} \\ \widehat{\eta} \end{array}\right\},$$

where the wavenumber α is a positive, real number, and $\hat{\imath} = \sqrt{-1}$ is the imaginary unit. The *exponential time factor* λ embodies the decay (or growth) characteristics of each solution mode. One such solution must be found for u, v and p on each of the three subdomains $\Omega_0^\pm$ and Ω_0^ϵ. If we substitute these expressions into Eqs. (12) and (13) on $\Omega_0^\pm$ (where the force term is zero), Stokes' equations reduce to systems of ODEs with solutions:

$$\widehat{p}^{\pm}(y) = A^\pm e^{\mp\alpha y}, \tag{16a}$$

$$\widehat{u}^{\pm}(y) = B^\pm e^{\mp\beta y} - \frac{\hat{\imath}\alpha}{\rho\lambda}A^\pm e^{\mp\alpha y}, \tag{16b}$$

$$\widehat{v}^{\pm}(y) = \pm\frac{\hat{\imath}\alpha}{\beta}B^\pm e^{\mp\beta y} \pm \frac{\alpha}{\rho\lambda}A^\pm e^{\mp\alpha y}, \tag{16c}$$

where β is a new parameter defined by $\beta^2 := \alpha^2 + \frac{\rho}{\mu}\lambda$ with $\mathscr{R}e(\beta) \geq 0$.

On the smoothing region, however, the integral forcing terms lead to a system of coupled integro-differential equations. After linearising the delta function terms (see [22] for details), these equations reduce

to:

$$\left(\rho\lambda + \mu\alpha^2 - \mu\frac{d^2}{dy^2}\right)\widehat{u}^\epsilon + \hat{\imath}\alpha\widehat{p}^\epsilon = -\sigma_t\theta\alpha^2\mathscr{D}_\alpha^\epsilon\widehat{\xi}\,d_\epsilon(y), \tag{17a}$$

$$\left(\rho\lambda + \mu\alpha^2 - \mu\frac{d^2}{dy^2}\right)\widehat{v}^\epsilon + \frac{d\widehat{p}^\epsilon}{dy} = -\sigma_n\theta\alpha^2\mathscr{D}_\alpha^\epsilon\widehat{\eta}\,d_\epsilon(y), \tag{17b}$$

$$\hat{\imath}\alpha\widehat{u}^\epsilon + \frac{d\widehat{v}^\epsilon}{dy} = 0, \tag{17c}$$

$$\lambda\widehat{\xi} = \mathscr{D}_\alpha^\epsilon\int_{-\epsilon}^{\epsilon}\widehat{u}^\epsilon(y)\cdot d_\epsilon(y)\,dy, \tag{17d}$$

$$\lambda\widehat{\eta} = \mathscr{D}_\alpha^\epsilon\int_{-\epsilon}^{\epsilon}\widehat{v}^\epsilon(y)\cdot d_\epsilon(y)\,dy. \tag{17e}$$

The expression $\mathscr{D}_\alpha^\epsilon$ arising in the above equations is the Fourier transform of the smoothed delta function, which for the cosine approximation is

$$\mathscr{D}_\alpha^\epsilon := \int_{-\epsilon}^{\epsilon} e^{\hat{\imath}\alpha r}d_\epsilon(r)\,dr = \frac{\pi^2\sin(\alpha\epsilon)}{\alpha\epsilon\left(\pi^2 - \alpha^2\epsilon^2\right)}.$$

At first glance, the coupled system (17a)–(17e) might appear too complicated to solve analytically, since the fibre positions are integrals of $\widehat{u}^\epsilon$ and $\widehat{v}^\epsilon$, while the velocity components are in turn solutions of differential equations with $\widehat{\xi}$ and $\widehat{\eta}$ on the right hand side. Fortunately, our situation is aided considerably by the fact that $\widehat{\xi}$ and $\widehat{\eta}$ are constants. Therefore, (17a)–(17c) may be solved for the velocity and pressure without knowing the fibre positions *a priori*. The resulting $\widehat{u}^\epsilon$ and $\widehat{v}^\epsilon$ are substituted into (17d) and (17e), yielding expressions for $\widehat{\xi}$ and $\widehat{\eta}$, which are then used to find the velocity. This procedure involves extensive algebraic manipulations, and is tractable only through the use of the symbolic algebra package Maple [4]. Unlike the solutions (16a)–(16c) on $\Omega_0^\pm$, the final expressions for the solution components are extremely lengthy, and so they are not presented here.

At this point, we have expressions for the solution components on three regions, each involving several unknown constants of integration. On $\Omega_0^\pm$, Eqs. (16a)–(16c) involve the four coefficients $A^\pm$ and $B^\pm$. The solution on the strip Ω_0^ϵ introduces an additional four constants of integration from the solution of Stokes' equations. In order to determine the solution uniquely, we must come up with a further eight conditions relating the eight constants, which arise quite naturally from matching the solutions at the interfaces $y = \pm\epsilon$. Four conditions ensue from the requirement that the pressure, velocities, and normal derivative $d\widehat{u}/dy$ be continuous at the interface $y = \epsilon$, and the remaining constraints arise from the same four continuity conditions at $y = -\epsilon$.

The resulting system of equations is linear and homogeneous, and so there is a non-trivial solution only if the determinant of the 8×8 coefficient matrix is zero. This determinant condition is simply a *dispersion relation*, giving λ in terms of α. It is too large to write in its entirety, but can be written symbolically in the compact form

$$S_n^\epsilon(\beta)\cdot S_t^\epsilon(\beta) = 0. \tag{18}$$

The subscripts n and t on the two factors in (18) corresponds to the fact that the fibre force parameter σ_n appears only in the factor $S_n^\epsilon(\beta)$, while $S_t^\epsilon(\beta)$ depends on σ_t only. While not indicated explicitly, it should be clear that $S_n^\epsilon(\beta)$ and $S_t^\epsilon(\beta)$ are also functions of the parameters α, ρ and μ.

We can make the following observations regarding the structure of the dispersion relation in comparison to the results for the unsmoothed problem from [24]:

- the structure of the dispersion relation is very similar in that there is a decoupling between the normal and tangential fibre modes.

– the dispersion relation is not a polynomial (as it was for the jump problem), since the factors in Eq. (18) involve trigonometric and exponential functions of the parameters. Consequently, there is no analytical expression for the solutions β and our only recourse is to apply a numerical root-finding technique such as Newton's method.

– the presence of exponential terms in the dispersion relation make the equation very ill-conditioned, particularly for large values of the forcing parameters σ_n and σ_t. The Newton solver requires a careful rescaling of the dispersion relation in conjunction with quadruple precision arithmetic, and continuation in ϵ.

For the jump problem, we were able to prove in [22] that the fibre modes are stable (that is, $\mathscr{R}e(\lambda) < 0$ for all real α), and we also compared the values of λ over a wide range of parameters. However, the smoothed dispersion relation (18) is more complex and ill-conditioned, and hence it is much more difficult to determine the roots. Nevertheless, we will see in the following section that we can obtain solution modes for the smoothed problem with factors λ that are more representative of the decay behaviour of immersed fibres observed in computations.

3.3 Stability and stiffness of fibre modes

In order to make these results as applicable as possible to previous work, we have chosen representative parameter values from computations reported in the literature for biological applications (primarily from [16], [6] and [17]). We will choose $\rho = 1.0\ g/cm^3$ and the forcing parameter σ to lie between 10^4 and $10^6\ g/cm \cdot sec^2$, where $\sigma \equiv \sigma_n = \sigma_t$. The viscosity used in typical biological applications (such as flagella in intra-cellular fluid) is $\mu = 1.0\ g/cm \cdot sec$, while that for blood is $0.04\ g/cm \cdot sec$. However, most immersed boundary simulations of the heart and arteries have been forced to take $\mu = 1.0$ in order to avoid limitations on the time step. The domain is a square with sides of length $1\ cm$, on which is laid a 64×64 computational grid, and the fibre is discretised at 196 points; i.e. $N = 64$, $\epsilon = \frac{2}{64}$ and $N_b = 196$.

It is important to keep in mind that the procedure outlined in the previous section does not yield a formula for an exact solution that can compared directly with computations — the equations are too complicated even for MAPLE to yield explicit formulas for the solution components. What we aim to investigate instead is the behaviour of a particular set of modes, represented as pairs (α, λ), which arise from solutions of the dispersion relation (18). Consider a discrete set of wavenumbers, $\alpha = 2\pi \cdot i$, $i \in \{1, 2, \ldots, N\}$, corresponding to the modes that can be resolved on an equally-spaced grid with mesh spacing $h = \frac{1}{N}$ in the x–direction. By restricting α in this manner, we are still dealing with the continuous equations but have discretised the problem *in an idealised sense*. We also choose the smoothing length $\epsilon = \frac{2}{N}$ to agree with the radius of support for the delta function in the immersed boundary method.

Stability. For all wavenumbers and parameter ranges that we have considered, the solution modes arising from the dispersion relation exhibit a decay rate with negative real part; that is, $\mathscr{R}e(\lambda) < 0$. While this is not as strong a result as the stability proof presented in [22] for the jump formulation of the problem, it still provides compelling evidence that the smoothed fibre modes are also stable in time.

Stiffness. The stiffness of the immersed fibre problem is characterised by the size of the complex eigenvalues λ. A large variation in the magnitude of the real part $\mathscr{R}e(\lambda)$ indicates a solution with components that decay on widely-varying time scales; correspondingly, a large variation in $\mathscr{I}m(\lambda)$ points to modes with disparate frequencies of oscillation. In both cases, the problem is distinguished by a mixture of time scales that differ is size by orders of magnitude: any computation based on such a problem requires the use of stiff solvers.

By examining the decay rates $\mathscr{R}e(\lambda)$, and frequencies of oscillation $\mathscr{I}m(\lambda)$, we can identify the stiffness characteristics of the underlying solution, and how they depend on the parameters. Table I summarizes the maximum values of λ for the jump and smoothed formulations of the problem, with $\sigma = 10^5$ representative of the range of forcing parameters encountered in physical problems. The *"Stokes modes"* correspond to solutions of Stokes' equations without an immersed fibre, for which $\lambda^S = -\frac{\mu}{\rho}\alpha^2$. Let us begin by comparing

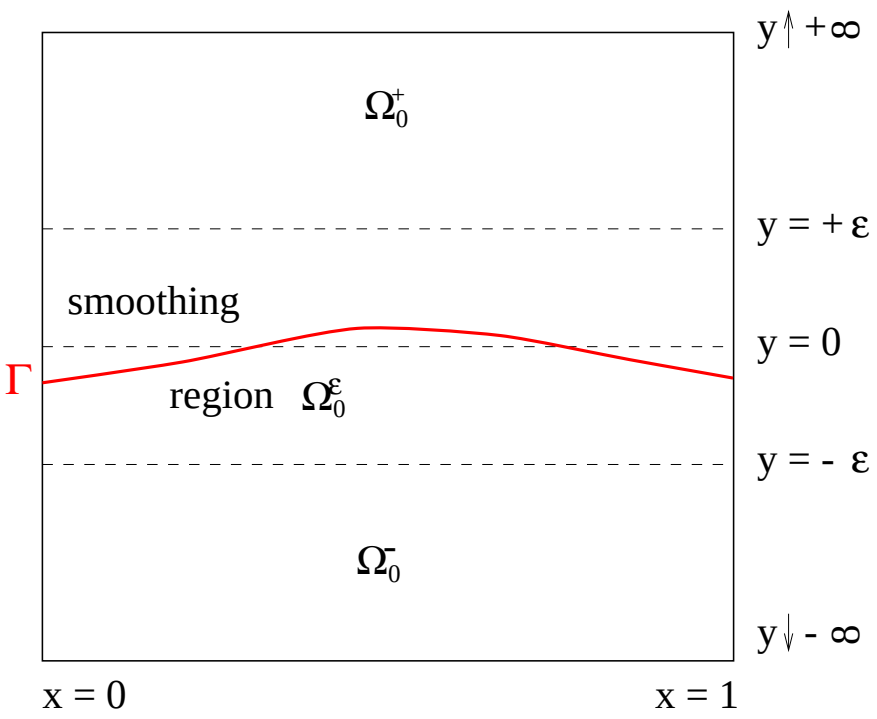

Figure 3: A blow-up of the region Ω_0 in Fig. 1, with the fibre at equilibrium along $y = 0$, and the smoothing region Ω_0^ϵ, of width 2ϵ.

Table I: Comparison of the maximum λ for solution modes of Stokes' equations, the jump formulation and the smoothed problem with $\sigma = 10^5$.

	$\mu = 0.04$		$\mu = 1.0$	
	$\max \lvert \mathscr{R}e(\lambda) \rvert$	$\max \lvert \mathscr{I}m(\lambda) \rvert$	$\max \lvert \mathscr{R}e(\lambda) \rvert$	$\max \lvert \mathscr{I}m(\lambda) \rvert$
Stokes modes	6.4×10^3	0.0	1.6×10^5	0.0
Fibre modes (jump)	5.7×10^6	9.6×10^6	6.3×10^5	9.0×10^5
Fibre modes (smooth)	6.0×10^3	3.3×10^4	5.9×10^4	1.3×10^4

the solutions to Stokes' problem and the "jump" problem with the exact delta function (taken from [22]), from which it is clear that the presence of an immersed fibre affects the rate of decay of solution modes considerably, while also introducing significant oscillatory features in the solution. The fibre therefore introduces a certain degree of stiffness in the problem, which translates numerically into a stricter requirement on the time step in the immersed boundary method. The magnitude of λ increases by a factor of 7 when $\mu = 1.0$, and by almost 2000 for the smaller value of viscosity. It is here that the unsmoothed analysis over-predicts the stiffness observed in computations. The maximum allowable time step typically depends inversely on the magnitude of the solution modes λ, from which the first two rows of Table I suggest that immersed boundary computations should require a time step orders of magnitude smaller than that for Stokes flow without a fibre. On the contrary, numerical evidence shows that the time step restrictions are comparable for this moderate value of the fibre force parameter, even when μ is as small as 0.04.

This discrepancy can be attributed to exclusion of smoothing effects in the jump formulation of the problem. The final row of Table I indicates that the smoothed modes are more comparable in size with the Stokes modes, and hence more in line with what is seen in actual computations for this example. Nevertheless, the appearance of a large imaginary part in the modes translates into a considerable degree of stiffness, which is also observed in computations for this parameter range. Fig. 4 gives a pictorial representation of the effect of smoothing on the entire discrete spectrum of fibre modes. Replacing the delta function with a smoothed

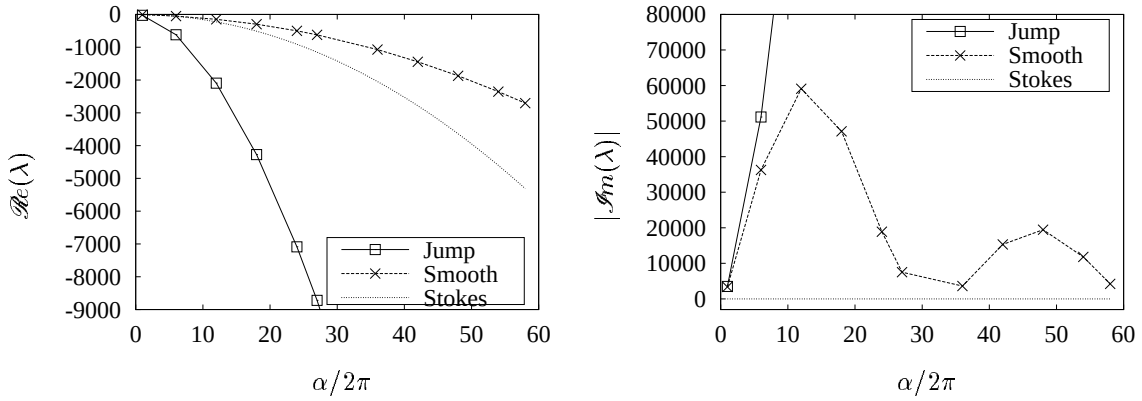

Figure 4: A comparison of $\mathscr{R}e(\lambda)$ and $\mathscr{I}m(\lambda)$ for the jump and smoothed dispersion relations with $\alpha \in [2\pi, 128\pi]$, $\mu = 0.04$ and $\sigma = 10^5$.

approximation clearly has a profound effect on the decay and frequency characteristics of an immersed fibre, particularly for the larger wavenumbers. However, it appears that the lowest wavenumber modes (with $\alpha = 2\pi$) match quite well between the two problems, which suggests that the dominant solution features are relatively unchanged by smoothing. Numerical verification of this consistency is given below.

It is interesting to compare the size of solution modes in terms viscosity in Table I. While a reduction in μ decreases the stiffness of the Stokes problem considerably, the smoothed fibre modes are affected to a much lesser degree, with the modes only decreasing by a factor of two in size, and the imaginary part actually becoming larger (the implications of this behaviour for time-stepping will become obvious in the next section). On the other hand, the dependence of the fibre modes on σ is much stronger, with the stiffness of the problem worsening significantly as the forcing parameter is increased. The σ dependence was not included in Table I, since a detailed discussion of the effect of σ and μ on the time step restrictions, along with comparisons to actual computations, will be given in Section 4.

Finally, we observed without exception that the largest growth rates arose from the *tangential* term in dispersion relation, with the normal modes being smaller and similar in magnitude to Stokes' modes. This is consistent with the asymptotic result our previous work which showed that the normal fibre modes are similar in magnitude to Stokes modes in the large σ limit [24]. Therefore, the stiffness in the problem may

be traced to tangential oscillations of the immersed fibre. It is very possible that the decoupling of the fibre modes may be exploited to develop more efficient numerical solvers, perhaps using some form of rescaling or preconditioning based on a local linearisation near the fibre which singles out the tangential motions.

Quantitative comparisons. While the previous discussion of stiffness and stability is very useful in understanding the qualitative behaviour of fibre modes, it offers little in the way of quantitative information about actual solution behaviour or decay rates. Rather than looking at a range of wavenumbers corresponding to all modes resolvable in an idealised discretisation of the problem, we can instead focus on the dominant solution features represented by the lowest wavenumber ($\alpha = 2\pi$) mode. We expect that the higher frequency oscillations in any computation should die out most rapidly, leaving only the lowest frequency mode after a short initial time period.

A simple model problem can be used to test this hypothesis. Consider a single immersed fibre, such as that pictured in Fig. 3, which is periodic in the x–direction and initially has a sinusoidal perturbation with small amplitude. This fibre will oscillate about its horizontal rest state decaying in time toward zero. By measuring the height of the maxima in each oscillation, as well as the period of the motion, we can obtain values for the real and imaginary part of the dominant computed solution mode with which to compare to our theoretical predictions from the roots of the dispersion relation for the smoothed problem. The results are summarised in Table II, from which it is clear that dominant solution characteristics are captured quite well by computations at least when the fibre forcing parameter, σ, is small. When σ is increased, the predicted

Table II: A comparison of the predicted and computed decay rates and frequencies for the lowest wavenumber modes, $\alpha = 2\pi$, for the jump and smoothed delta function formulations ($\mu = 1.0$).

σ	Smallest decay rate $\mathscr{R}e(\lambda)$			Frequency $\mathscr{I}m(\lambda)$		
	Analytical (jump)	Analytical (smooth)	Computed	Analytical (jump)	Analytical (smooth)	Computed
10^2	−33	−33	−32	86	85	85
10^3	−51	−50	−46	310	307	310
10^4	−84	−76	−75	1040	1025	1030
10^5	−142	−108	−131	3390	3320	3360

λ compares less favourably with the computed values, but still remains within approximately 10%.

It is interesting to compare the predictions from the jump and smooth formulations, which are quite close particularly for the smaller values of σ. If we also include the effect of varying the smoothing radius, we see in Table III that the dominant mode of the smoothed solution tends toward that of the jump problem as ϵ is reduced in size. This is further evidence of the consistency between the smoothed and unsmoothed problems, and shows that while smoothing may dominate the higher frequency modes (as observed earlier in Fig. 4), it has much less influence on the main features of the solution, particularly when ϵ is small.

Table III: A comparison of the analytical decay rates for the lowest wavenumber mode ($\alpha = 2\pi$) for varying smoothing radius ($N = 64$).

σ	Smallest Decay Rate							
	Jumps	$\epsilon = \frac{1}{64}$	$\epsilon = \frac{2}{64}$	$\epsilon = \frac{3}{64}$	$\epsilon = \frac{4}{64}$	$\epsilon = \frac{5}{64}$	$\epsilon = \frac{6}{64}$	$\epsilon = \frac{7}{64}$
10^2	−33	−33	−33	−33	−32	−32	−31	−31
10^3	−51	−51	−50	−48	−46	−44	−42	−40
10^4	−84	−81	−76	−69	−62	−57	−52	−48
10^5	−142	−129	−108	−89	−75	−64	−57	−51

4 Time-stepping schemes

The linear analysis of the preceding section showed that the fibre modes capture the qualitative behaviour manifested in computations, provided the smoothing effects of the delta function approximation is taken into account. We will now use these stiff fibre modes to explain the severe time step restriction on immersed boundary computations in which the fibre is treated explicitly (by *"explicit"*, we refer to time discretisations that treat the fibre position and the fibre force term in the Navier-Stokes equations explicitly, regardless of whether diffusion and pressure are treated implicitly or explicitly). As we will see in Section 4.1, it is in fact the fibre forcing terms that govern the time step in explicit computations. The *FE/BE* scheme outlined in Section 2.2, which is also the most commonly-used approach, couples the pressure and diffusion implicitly in a Stokes solve while treating the fibre terms explicitly.

The severe stiffness arising from the immersed boundary problem and the correspondingly strict time step limit in computations have been well-documented in the literature [16, 26]. As a result, the importance of dealing with the immersed fibres in an implicit fashion is obvious, and a great deal of effort has gone into developing variations of the method that couple the fibre terms in the equations implicitly with the fluid. We have separated the various methods into the following four classes, based on the manner in which the fibre force term and fibre evolution equation are discretised:

A. Explicit: schemes that are explicit in the fibre force and position, and yet couple the diffusion terms implicitly (that include the *FE/BE* scheme of Section 2.2). The vast majority of recent computations couple diffusion and convection implicitly by combining an ADI step with a pressure projection step. More recently, it has been recognised that convection is not so important in relation to the stiffness arising from the fibre, and the fluid equations have been solved using a couple Stokes solver, while treating convection terms explicitly using upwind differencing [18, 15].

B. "Approximate implicit": a scheme that couples the fibre force with the fibre evolution equation to form an iteration on the fibre position that is independent of the fluid unknowns [16]. Once the iteration has converged, the *intermediate* or *predicted fibre position* is used to compute the fibre force in the fluid equations, which are then solved using the same techniques as for the explicit schemes. While this is not truly an implicit scheme (and hence the name), the iteration helps to prevent violent instabilities in fibres with extremely large force parameters. Fogelson & Peskin [8] developed an alternate formulation of this class of iterative schemes in terms of minimising an energy functional for the fibre position.

C. Semi-implicit: refers to schemes that couple the fibre with the fluid unknowns in an iterative fashion, such as the method proposed by Mayo & Peskin [13].

D. Fully implicit: where the fibre and fluid unknowns are solved simultaneously. Tu & Peskin implemented a fully implicit solver for Stokes flow [26], and showed that while it appeared to be unconditionally stable, this scheme was far too expensive for practical computations.

It is approaches A and B that have been used most often in practice, with the majority of recent computations using the explicit technique A. While the "approximate implicit" scheme does help to ease the severe stability restrictions in problems with extremely large σ, it is our experience that the added cost of the iteration embedded in each time step essentially wipes out any advantage that would have been gained by taking larger time steps. The predominance of explicit schemes, which are extremely simple to program, is thus not surprising.

Nonetheless, the stability restrictions on explicit computations persist, and remain a serious limitation on the problems that can be simulated numerically. We have shown that the stiffness arises not from Reynolds number effects, but rather from a large fibre forcing parameter. While implementing a better fluid solver might provide improved resolution of the fine-scale boundary layer effects present in high Reynolds number (convection-dominated) flows, it will not help deal with the stiffness in immersed boundary computations arising from the fibre forcing terms, which we have shown are present even in the absence of convection. On the contrary, it is essential that more efficient implicit (or semi-implicit) schemes be developed which deal specifically with the stiffness that dominates computations when the fibre forcing term is large.

In this section, we will concentrate our attention on the explicit and semi-implicit schemes. The fibre modes derived in the last section will be used to predict stability restrictions for various explicit time-stepping schemes, using a straightforward application of stability diagrams. The family of Runge-Kutta schemes exhibit the most desirable properties of explicit schemes, and we briefly describe a class of semi-implicit schemes, similar to the *FE/BE* method, but which use an Implicit-Explicit Runge-Kutta (or *IMEX-RK*) approach instead. Finally, we demonstrate how our modal analysis can be extended to time discrete problems, and this technique will be applied to the Mayo-Peskin method in order to estimate convergence rates for the iteration.

4.1 Explicit schemes

In the following discussion, we distinguish between the solution modes arising from an idealised discretisation of the smoothed fibre, and those from Stokes flow without an immersed boundary, since the time step in a discretisation of the immersed fibre problem is limited by a combination of diffusive and fibre effects. Fig. 5 depicts the relative size of both sets of solution modes in the λ–plane, for $\sigma = 10^4$ and 10^6, with the Stokes modes marked "$*$" and fibre modes "$\circ$" (note that these correspond to the complete set of modes for the results presented earlier in Table I). The solid curves represent the boundary of the region of absolute stability for a Forward Euler discretisation (based on the Stokes modes), while the maximum time step allowed by Forward Euler for both sets of modes (denoted k^* and k°) are listed on each plot for easy comparison of the stability limits. Fig. 5(a), corresponding to $\mu = 1.0$, demonstrates that the time step restriction for a fibre force of $\sigma = 10^4$ is comparable to that experienced in the absence of the fibre. When σ is increased to 10^6 in Fig. 5(b), the modes migrate outward along the imaginary axis, requiring a much smaller time step. A similar heightening of stiffness is observed when the viscosity is decreased, as shown in the remaining plots in Figs. 5(c) and (d) for the much lower viscosity of $\mu = 0.04$.

It is precisely this parameter regime, corresponding large fibre force and small viscosity, where immersed boundary computations have been observed to suffer the most difficulty. In fact, in numerous heart valve simulations reported in the literature [17, 19], a careful scaling argument was required to justify choosing $\mu = 1.0$ (instead of the actual viscosity of blood $\mu \approx 0.04$) in order for the time step requirement in computations to be practical. The most significant conclusion that can be drawn from this discussion is that the stiffness in the immersed boundary method arises from the interaction of the fibre and fluid, through a combination of large fibre force and small viscosity, rather than the high Reynolds number effects that limit typical fluid flow calculations for other problems not characterised by this fluid-structure interaction.

The above discussion pertains to a fully explicit discretisation of the problem and ignores any coupling between diffusion and fibre forcing, and so it is worthwhile to discuss for a moment how these results apply to the *FE/BE* method, which treats diffusion implicitly. Diffusive terms are invariably discretised in an implicit fashion, since it is well known that an explicit, centered, finite difference discretisation of diffusion gives rise to a stability restriction of the form

$$k \leq \frac{\rho h^2}{4\mu}.$$

This is unacceptable in ordinary fluid flow simulations because simple implicit schemes will eliminate the constraint on k, making the scheme unconditionally stable. However, the point we wish to make here is that even for the moderate fibre forcing parameter $\sigma = 10^4$, the restriction arising from handling fibre modes explicitly is nearly as bad as that from diffusion. This can be inferred from the fact that the modes pictured in Fig. 5(a) are very close to the border of the stability region. Furthermore, the fibre modes worsen significantly in relation to the Stokes modes when σ is increased. Therefore, it is essential to consider the behaviour of the fibre modes when designing any time-stepping strategy for the immersed fibre problem if one wishes to overcome this type of stability restriction. The most obvious approach is to perform an implicit discretisation of the fibre terms in the equations, but this is particularly difficult in the case of the immersed fibre problem because of the nonlinear, nonlocal coupling of the fibre with the fluid.

Another simpler strategy is to search out different explicit schemes that deal more effectively with solution modes that tend to cluster near the imaginary axis. An obvious candidate for an alternative explicit time-

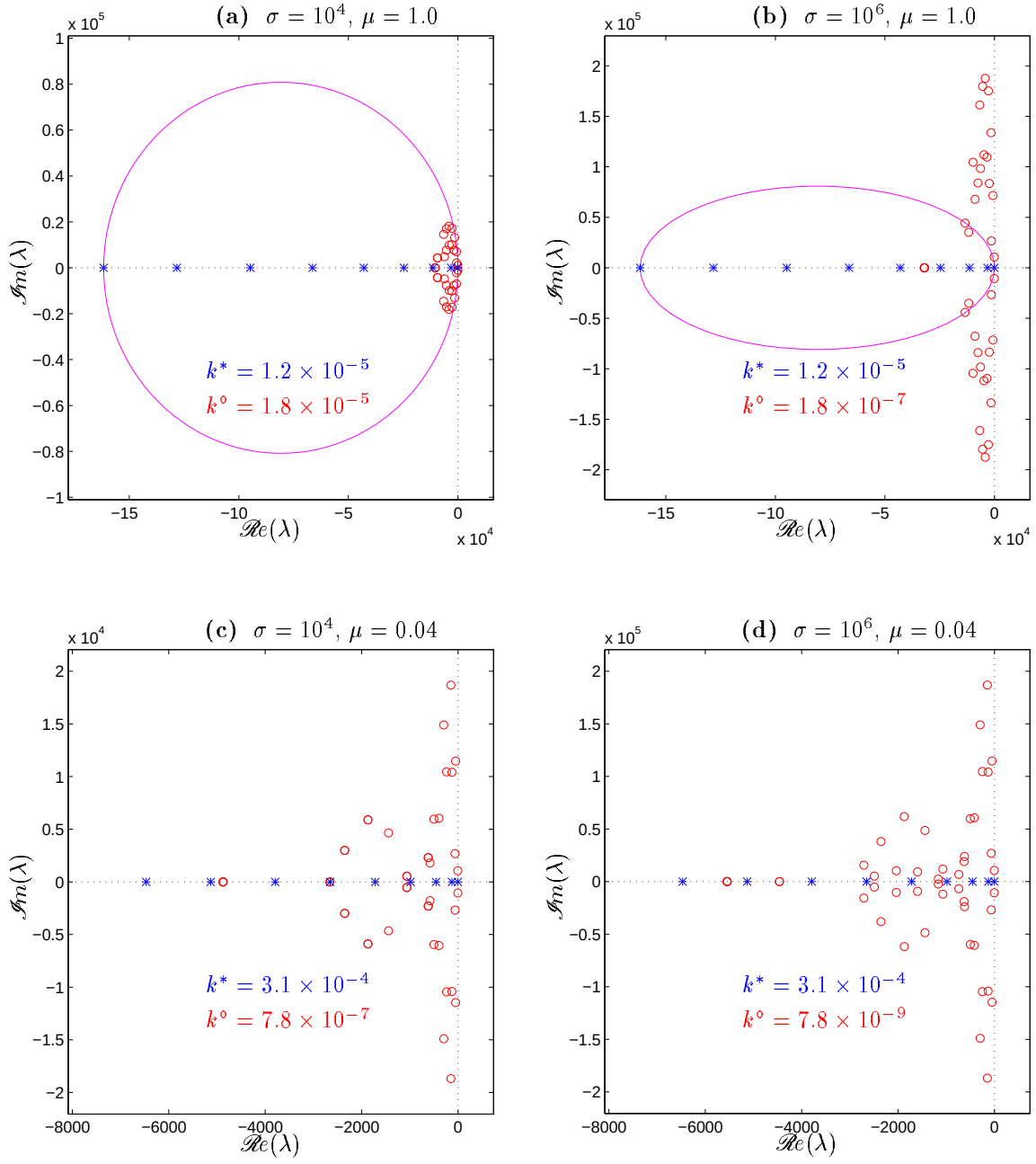

Figure 5: Region of absolute stability for the Forward Euler scheme, along with the smoothed fibre modes ($\circ$) and Stokes modes ($*$). The stability boundary, drawn as a solid line in plots (a) and (b), is computed based on the Stokes modes, while the maximum allowable time steps, k^* and k°, are listed for each set of modes. Note the difference in the axis scales between the four plots, and in particular the stretching of the vertical axis in (c) and (d).

stepping technique is the Runge-Kutta (RK) family of schemes. The regions of absolute stability for the RK methods of order one through four are pictured in Fig. 6, with the time step chosen to be the largest afforded by the *RK4* scheme, or $k = 6.0 \times 10^{-4}$. In this situation, our analysis suggests that the *RK1* method should

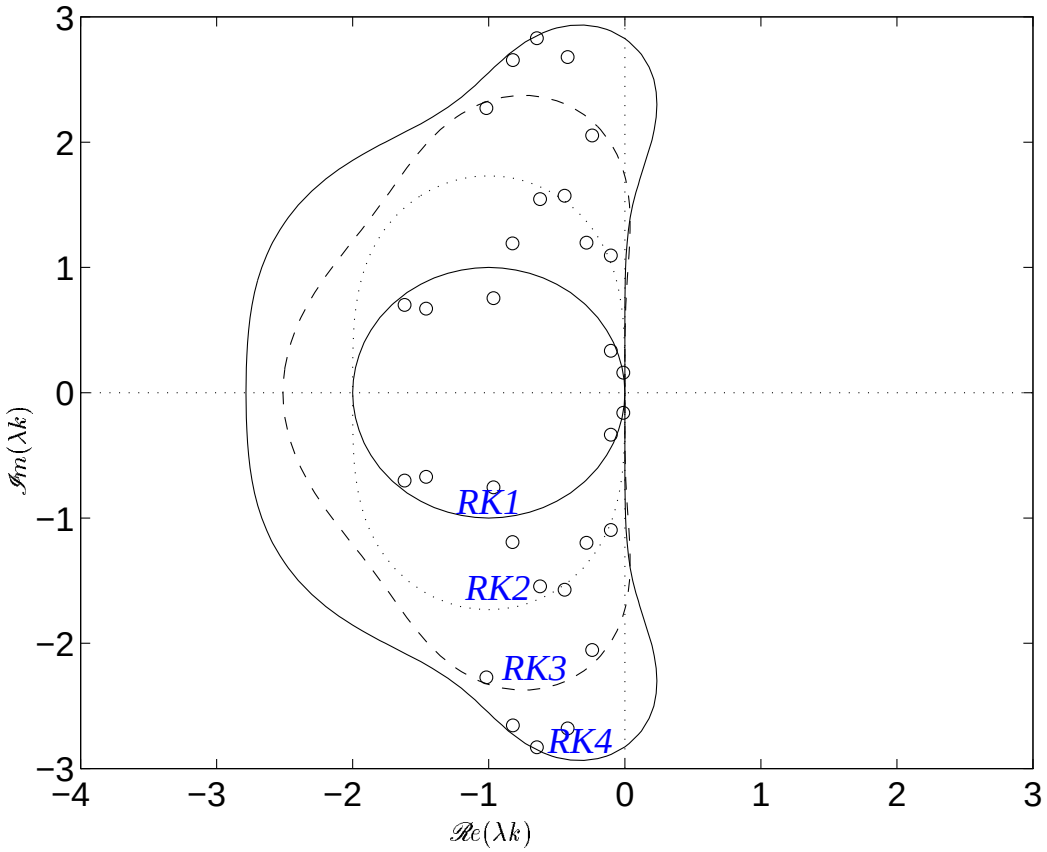

Figure 6: Regions of absolute stability for the explicit Runge–Kutta schemes of orders 1 through 4, along with the same set of fibre modes pictured in Fig. 5 for $\sigma = 10^4$.

require a time step 10 times smaller for the stability region to encompass all modes (which translates into a factor of 2.5 increase in efficiency after figuring in the cost of the four RK stages). As σ is increased even further, the fibre modes become more stiff and the superiority of *RK4* asserts itself.

These predictions for the fully explicit methods are confirmed by the computations presented in Fig. 7. We can see from the plots of maximum time step for the various RK schemes (along with the accompanying CPU times in Table IV) that the *RK4* scheme is the best of all the explicit methods considered. The *FE/BE* restults are included for comparison purposes. While this semi-implicit approach is very similar to the *RK1* method, there is clearly a great deal of advantage to be gained from its implicit treatment of the diffusion term, about which more will be said in the next section.

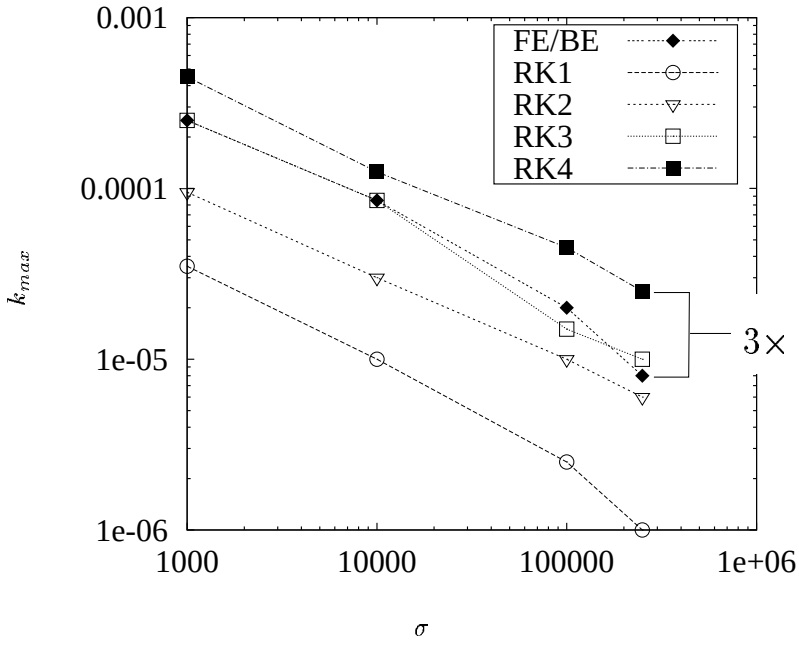

Figure 7: Comparison of computed time step restrictions for the Runge–Kutta schemes and the ADI implementation of the immersed boundary method, for $\mu = 0.01$.

Table IV: CPU times for the $\sigma = 2.5 \times 10^5$ computations in Fig. 7 (performed on an SGI Origin 2000 (4×195 MHz R10000 processors, 512 Mb RAM)).

Scheme	CPU Time Required (sec)	
	$\mu = 1.0$	$\mu = 0.01$
RK1	370.59	1658.21
RK2	138.12	143.02
RK3	110.87	99.44
RK4	109.76	52.64
FE/BE	53.96	54.12

4.2 Stability of the *FE/BE* scheme

We begin by rewriting the equations of motion and identifying which terms are discretised implicitly and explicitly:

$$\frac{\partial \boldsymbol{u}}{\partial t} = \underbrace{\frac{1}{\rho}\bar{\mathcal{S}}\sigma\frac{\partial^2 \boldsymbol{X}}{\partial s^2}}_{\text{explicit terms } \hat{g}(\boldsymbol{u})} + \underbrace{\frac{\mu}{\rho}\Delta\boldsymbol{u} - \frac{1}{\rho}\nabla p}_{\text{implicit terms } g(\boldsymbol{u})}, \tag{19}$$

$$\nabla \cdot \boldsymbol{u} = 0, \tag{20}$$

$$\frac{\partial \boldsymbol{X}}{\partial t} = \underbrace{\mathcal{S}\boldsymbol{u}}_{\text{explicit}}. \tag{21}$$

The symbols $\mathcal{S}$ and $\bar{\mathcal{S}}$ represent the delta function interpolation operators, which transfer between grid quantities $\boldsymbol{V}(\boldsymbol{x})$ and fibre grid quantities $\boldsymbol{W}(s)$ as follows:

$$\mathcal{S}\boldsymbol{V}(\boldsymbol{x}) = \int_\Omega \boldsymbol{V}(\boldsymbol{x}) \cdot \delta_\epsilon\left(\boldsymbol{x} - \boldsymbol{X}(s,t)\right) d\boldsymbol{x} \qquad \text{and} \qquad \bar{\mathcal{S}}\boldsymbol{W}(s) = \int_\Gamma \boldsymbol{W}(s) \cdot \delta_\epsilon\left(\boldsymbol{x} - \boldsymbol{X}(s,t)\right) ds.$$

If we discretise these equations in time only, using the *FE/BE* scheme described in Section 2.2, then we have

$$\boldsymbol{u}^n - \frac{k\mu}{\rho}\Delta\boldsymbol{u}^n + \frac{k}{\rho}\nabla p^n = \boldsymbol{u}^{n-1} + \frac{k}{\rho}\bar{\mathcal{S}}\sigma\frac{d^2}{ds^2}\boldsymbol{X}^{n-1}, \tag{22}$$

$$\nabla \cdot \boldsymbol{u}^n = 0, \tag{23}$$

$$\boldsymbol{X}^n = \boldsymbol{X}^{n-1} + k\mathcal{S}\boldsymbol{u}^n, \tag{24}$$

where we have abused notation somewhat by denoting semi-discrete quantities at time t_n (which are continuous in space only) by a superscript $(\cdot)^n$.

We now investigate the stability in time of the solutions to Eqs. (22)–(24) by assuming that $\boldsymbol{u}^n$ and $\boldsymbol{X}^n$ depend on the solutions at the previous time step as

$$\boldsymbol{u}^n = \gamma\boldsymbol{u}^{n-1} \qquad \text{and} \qquad \boldsymbol{X}^n = \gamma\boldsymbol{X}^{n-1},$$

where γ is the *amplification factor*, which replaces $e^{\lambda t}$ from the time-continuous analysis. Again, we look for separable solutions of the form

$$\begin{Bmatrix} \boldsymbol{u} \\ p \\ \boldsymbol{X} \end{Bmatrix}^n = e^{\hat{\imath}\alpha x} \begin{Bmatrix} \widehat{\boldsymbol{u}}(y) \\ \widehat{p}(y) \\ \widehat{\boldsymbol{X}} \end{Bmatrix}^n. \tag{25}$$

On substituting these expressions into the time-discrete equations, we obtain a system of ODEs for the solution components as functions of y. It should be clear to the reader that the solution process is nearly identical to that described in Section 3.2, and so we omit the details of the derivation. At the end, we obtain a dispersion relation which gives the amplification factor in terms of the other parameters in the problem. The *FE/BE* scheme is stable provided that all γ arising from this equation satisfy $|\gamma| < 1$.

As before, we apply a Newton iteration, with continuation in the smoothing radius ϵ, to solve the dispersion relation over a range of time steps and for all wavenumbers $\alpha/2\pi \in [1, 64]$. The character of the amplification factors is exactly what we would expect given our previous experience with the modal analysis of the continuous problem. We summarise the key points below:

- for time steps below a certain critical value, $k < k_{max}$, all roots satisfy $\gamma < 1$.

- for $k \geq k_{max}$, there are some γ greater than 1, indicating modes that are unstable in time, and which invariably correspond to the lower half of the spectrum, with the peak at $\alpha/2\pi \approx 10$. Furthermore, the modes in the upper half of the spectrum, $32 < \alpha/2\pi < 64$, are stable for the parameters under consideration here.
- when σ is increased, the number of unstable modes and the size of the amplification factor for these modes both increase.
- the largest amplification factor, and the first to become unstable, corresponds to a tangential mode of oscillation in the fibre.

The critical time step k_{max} is given in Table V for various forcing parameters, with the corresponding time step limit observed in computations with the same fibre force. In all cases, our analysis predicts a k_{max} which

Table V: A comparison of the maximum time step predicted by the theory and observed in computations for the *FE/BE* method, with $N = 64$, $\epsilon = \frac{1}{64}$, $\mu = 1$.

σ	k_{max} (predicted)	k_{max} (computed)
10^2	4×10^{-3}	8×10^{-3}
10^3	2×10^{-4}	6×10^{-4}
10^4	6×10^{-5}	1×10^{-4}
10^5	8×10^{-6}	2×10^{-5}

is consistently one-half as large as the actual time step limit encountered in computations. Considering the approximations that have been made in our "idealised discretisation," this discrepancy is not surprising.

4.3 Semi-implicit, iterative schemes

Instead of solving Eqs. (22)–(24) in a two-step process, Mayo & Peskin build an iterative scheme around this system [13], in order to couple the fibre evolution equation with the solution of the fluid equations. In essence, this involves replacing quantities $(\cdot)^n$ at time level n with values $(\cdot)^{n,m}$, where m refers to the iteration number. The only significant change, which is what couples the equations into an iteration, is that $\boldsymbol{X}^{n-1}$ in Eq. (22) is replaced with $\boldsymbol{X}^{n,m-1}$. We make a change of notation here, and write the Stokes solve represented by Eqs. (22) and (23) symbolically using the operator $\mathcal{H}$ as

$$\boldsymbol{u}^{n,m} = \mathcal{H}\left(\boldsymbol{u}^{n-1} + \frac{k}{\rho}\bar{\mathcal{S}}\sigma\frac{d^2}{ds^2}\boldsymbol{X}^{n,m-1}\right),$$
$$\boldsymbol{X}^{n,m} = \boldsymbol{X}^{n-1} + k\mathcal{S}\boldsymbol{u}^{n,m}.$$

By substituting the expression for $\boldsymbol{u}^{n,m}$ into the fibre evolution equation, the iteration may be written as a single equation for $\boldsymbol{X}$:

$$\boldsymbol{X}^{n,m} = \underbrace{\boldsymbol{X}^{n-1} + k\mathcal{S}\mathcal{H}\boldsymbol{u}^{n-1}}_{\boldsymbol{Z}^{n-1}} + \mathcal{S}\mathcal{H}\bar{\mathcal{S}}\underbrace{\frac{\sigma k^2}{\rho}\frac{d^2}{ds^2}}_{\mathcal{A}}\boldsymbol{X}^{n,m-1},$$

which can be written more compactly as

$$\boldsymbol{X}^{n,m} = \boldsymbol{Z}^{n-1} + \mathcal{S}\mathcal{H}\bar{\mathcal{S}}\mathcal{A}\boldsymbol{X}^{n,m-1}. \tag{26}$$

In practice, this iteration converges very slowly, and the convergence is speeded considerably by using the modified iteration

$$(\mathcal{I} - \mathcal{D}\mathcal{A})\left(\boldsymbol{X}^{n,m} - \boldsymbol{X}^{n,m-1}\right) = \boldsymbol{Z}^{n-1} - (\mathcal{I} - \mathcal{S}\mathcal{H}\bar{\mathcal{S}}\mathcal{A})\boldsymbol{X}^{n,m-1}, \tag{27}$$

which clearly has the same solution as (26). $\mathcal{I}$ signifies the identity operator, and $\mathcal{D} = \mathcal{S}\bar{\mathcal{S}}$ is a scaling factor. In the fully discrete setting, $(\mathcal{I} - \mathcal{S}\mathcal{H}\bar{\mathcal{S}}\mathcal{A})$ is a dense matrix, while $(\mathcal{I} - \mathcal{D}\mathcal{A})$ is a block tridiagonal preconditioner which accelerates convergence.

To quantify the rate of convergence, we again look for solutions of the form $\boldsymbol{X}^{n,m} = e^{\xi\alpha x}\widehat{\boldsymbol{X}}^{n,m}$ on each of the subdomains $\Omega_0^{\pm}$ and Ω_0^{ξ}, and solve the resulting system of ODEs as before. While the solution procedure is very similar to what we have seen already, it is important to realise that there is one very significant difference from the continuous problem: rather than the fluid force being defined implicitly in terms of the fibre position, the force is computed *based on the fibre position from the previous iteration.* Consequently, the semi–discrete analogue of the fibre iteration (27) is a formula for $\widehat{\boldsymbol{X}}^{n,m}$ in terms of $\widehat{\boldsymbol{X}}^{n,m-1}$.

Therefore, the solution procedure is streamlined considerably, and Eq. (27) reduces to an iteration of the form

$$\mathcal{B}\widehat{\boldsymbol{X}}^{n,m} = \mathcal{C}\widehat{\boldsymbol{X}}^{n,m-1} + \boldsymbol{R}^{n-1},$$

where $\mathcal{B}$ and $\mathcal{C}$ are 2×2 matrices, and $\boldsymbol{R}^{n-1}$ is a 2–vector with entries evaluated at the previous time step. Since we are only interested in the rate of convergence of the iteration, it is expedient for us to consider the difference between successive iterates

$$\boldsymbol{E}^{n,m} = \widehat{\boldsymbol{X}}^{n,m} - \widehat{\boldsymbol{X}}^{n,m-1},$$

which satisfies the recurrence

$$\boldsymbol{E}^{n,m} = \mathcal{M}\boldsymbol{E}^{n,m-1},$$

where $\mathcal{M} = \mathcal{B}^{-1}\mathcal{C}$ is an *iteration matrix.* The convergence properties of the iteration are manifested in the eigenvalues of $\mathcal{M}$, which can be found using MAPLE as

$$\varrho_t = \frac{\sigma_t \pi^4 k^2 \sin^2(\alpha\epsilon)\left(-\pi^4 + \pi^4 e^{-2\alpha\epsilon} + 5\epsilon^3\pi^2\alpha^3 + 3\epsilon^5\alpha^5 + 2\pi^4\epsilon\alpha\right)}{\alpha\epsilon\left(\alpha^2\epsilon^2 + \pi^2\right)^2\left(-4\epsilon^7\alpha^4 + 8\epsilon^5\alpha^2\pi^2 - 4\epsilon^3\pi^4 + 3\pi^4\sigma_t k^2\sin^2(\alpha\epsilon)\right)}, \tag{28}$$

$$\varrho_n = \frac{\sigma_n \pi^6 k^2 \sin^2(\alpha\epsilon)\left(-\pi^2 e^{-2\alpha\epsilon} + \epsilon^3\alpha^3 + \pi^2\epsilon\alpha + \pi^2\right)}{\alpha\epsilon\left(\alpha^2\epsilon^2 + \pi^2\right)^2\left(-4\epsilon^7\alpha^4 + 8\epsilon^5\alpha^2\pi^2 - 4\epsilon^3\pi^4 + 3\pi^4\sigma_n k^2\sin^2(\alpha\epsilon)\right)}. \tag{29}$$

Just as the solution of the continuous problem decoupled the fibre modes into normal and tangential oscillations, so also does the convergence of the semi–discrete scheme depend on two distinct eigenvalues, corresponding to normal and tangential forcing. The convergence of the scheme is thus governed by $\varrho_{max} = \max(|\varrho_t|, |\varrho_n|)$ — if $\varrho_{max} < 1$, the iteration converges, otherwise it diverges. A contour plot of ϱ_{max} is given in Fig. 8, for parameter values $\mu = 1$ and $\sigma = 10^4$. Based on the convergence rate for the linearised problem, we can make the following observations:

- The iteration always converges, which is to to be expected, since the scheme was proven to be unconditionally convergent in [13].
- There is a critical value of α given by

  $$\alpha_c \approx 0.09057685940 \cdot (2\pi N)$$

  at which $\varrho_n = \varrho_t$, found by equating (28) and (29), setting $\sigma_n = \sigma_t$ and $\epsilon = \frac{2}{N}$, and then solving for α. For the example given in the contour plot, we have $\alpha_c \approx 5.7969 \cdot 2\pi$, which is indicated in Figure 8 as a dashed vertical line. When $\alpha < \alpha_c$, the normal convergence rate ϱ_n is the largest, while for $\alpha > \alpha_c$ the convergence of the tangential modes (ϱ_t) is slowest. For a given time step, the slowest mode to converge is the tangential mode — therefore, just as the tangential modes provide the greatest contribution to the stiffness in the problem, so also do they govern the convergence of the *MP* iteration.

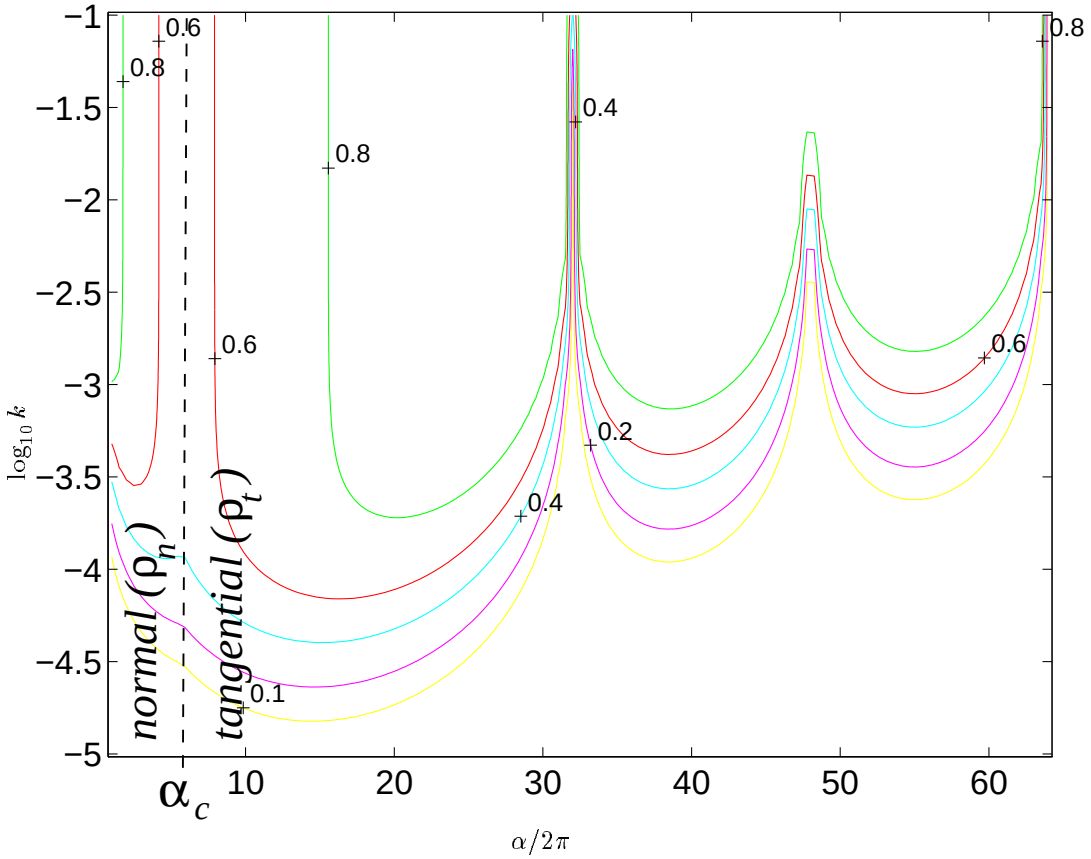

Figure 8: Convergence rate contours for the *MP* scheme. The vertical dotted line separates the parameter space into regions where the convergence rate for the normal mode (left) or the tangential mode (right) is largest ($\sigma = 10^4$).

Table VI: Predicted and computed convergence rates for the *MP* iterative scheme. The "—" entries correspond to instances where the scheme was unstable.

	$\sigma = 10^3$		$\sigma = 10^4$		$\sigma = 10^5$	
k	Pred.	Comp.	Pred.	Comp.	Pred.	Comp.
0.0001	0.01	0.01	0.08	0.08	0.43	0.43
0.0025	0.05	0.05	0.33	0.33	0.75	0.76
0.0005	0.17	0.18	0.62	0.62	0.84	—
0.0010	0.43	0.43	0.79	0.79	0.87	—
0.0025	0.75	0.73	0.86	—	0.88	—
0.0050	0.84	0.84	0.88	—	0.88	—

We also performed numerical experiments with the same model problem used in Section 3.3 in order to verify the predicted convergence rates, and the results are summarised in Table VI. The convergence rate was computed from the numerical results using the formula

$$Rate = \frac{Res^{m+1}}{Res^m},$$

where Res^m is the residual at iteration level m computed as follows:

$$Res^m = \left[\frac{1}{N_b} \sum_{\ell=0}^{N_b-1} \left\| \vec{X}_\ell^m - \vec{X}_\ell^{m-1} \right\|_2^2 \right]^{1/2}$$

and $\| \cdot \|_2$ is the standard L_2–norm on vectors. The predicted convergence rates were found by reading off ϱ_{max} for the dominant ($\alpha = 2\pi$) mode on the contour plot in Figure 8, which always corresponds to the normal fibre modes. Even though the tangential convergence rate is invariably the largest for the entire range of α in any given computation, and hence should dominate the convergence after a large number of iterations, they are also modes whose amplitude decays much more rapidly in time. Within every time step, however, only ten or so iterations were typically required to satisfy the residual tolerance, and so it is to be expected that the lowest wavenumber, normal modes will dominate the actual convergence rate observed in computations.

The blank entries in the table correspond to instances where the computation was unstable, which seems to go against our analytical predictions of unconditional convergence. However, we believe that this arises from a time instability which affects the numerical scheme when the time step is taken too large. In fact, Mayo & Peskin identify [13, p. 269] that even though their iteration scheme is convergent and is *more* stable in time than the fully explicit method, it is not *always* stable. While our analysis captures the convergence rate quite well, it is unable to predict onset of instability in computations.

4.4 Comparison

Before closing our discussion of time discretisations, we will draw a comparison between the explicit and semi-implicit approaches just described. We consider another test problem, which is more typical of that seen in the literature (see [26], [13] and [11]), in which the fibre is a closed loop which initially has the shape of an ellipse. As shown in Fig. 9, the semi–axes of the ellipse are of length 0.2 *cm* and 0.4 *cm*, and we use the same linear force density function with stiffness constant σ. The ellipse will tend toward an equilibrium state that is a circle with the same area as the original ellipse, because the fluid is incompressible — the radius of this final circle is approximately equal to 0.2828 *cm*. The reason for choosing this problem rather than the sinusoidally-perturbed flat fibre, is that the area (or "volume") of fluid inside the ellipse can be used as a measure of error in a given time-stepping scheme. Immersed boundary computations are known to experience loss of volume which becomes significant during more extreme flow conditions (large fibre force, pressure or velocity) such as those we are considering here. This volume loss problem was identified in [19] and shown to arise not from fluid passing physically through the immersed boundary, since the fibre points move along streamlines, but rather to the fact that the interpolated velocity field through which the immersed boundary moves is not discretely divergence–free. LeVeque & Li showed in [11] that the volume loss in the immersed boundary method for a problem nearly identical to our ellipse example grows linearly in time. Peskin & Printz [19] proposed a modified divergence stencil which reduces the volume loss significantly at the expense of an increase in the cost of delta function interpolation, though we have not implemented this modification in our simulations.

We applied the *RK1*, *RK4*, *FE/BE* and *MP* methods, and Table VII lists the maximum time steps and CPU times required for each method for two sets of computations with $\sigma = 10^4$ and 10^5, $\mu = \rho = 1.0$, $N = 64$ and $N_b = 192$. Among the fully explicit schemes, the *RK4* method is up to an order of magnitude more efficient than the Forward Euler (or *RK1*) scheme, and we see again that it is also competitive, in terms of CPU time, with the semi-implicit *FE/BE* method.

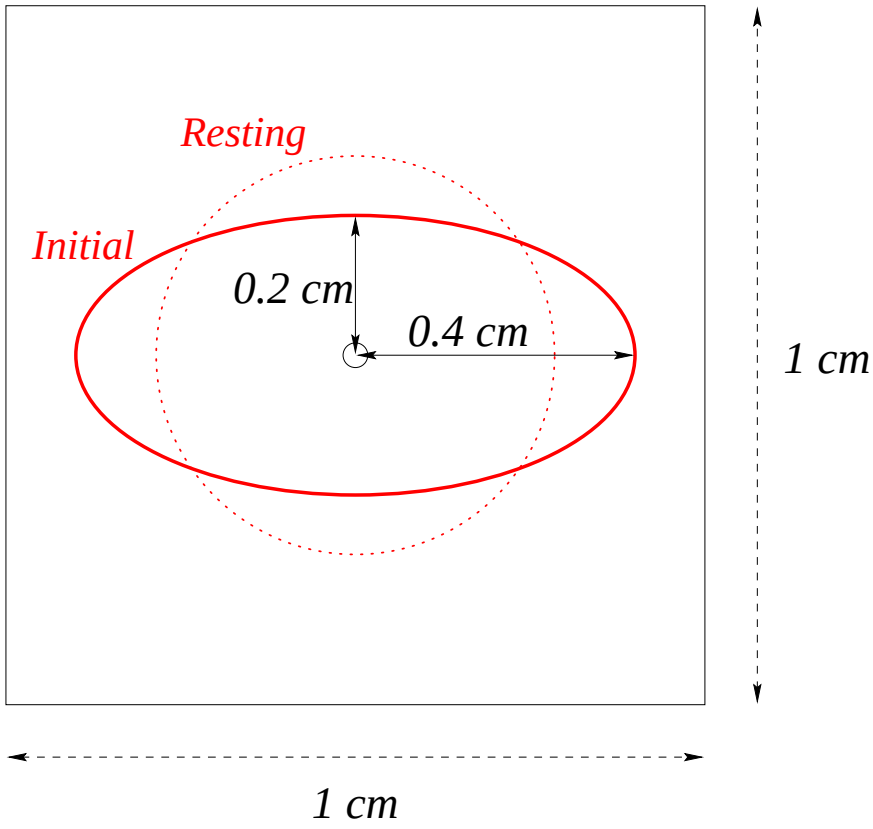

Figure 9: The "ellipse" test problem: the initial fibre position is an ellipse with semi–axes 0.4 cm and 0.2 cm. The equilibrium state is a circle with radius approximately 0.2828 cm.

Table VII: Comparison of computational cost for several explicit and semi–implicit schemes. The time step k_{max} was chosen to be the largest allowed by the method for stability, except for the MP scheme (which always converged). The "Vol. loss" is computed relative to the equilibrium value of 0.251 cm^2. CPU timings were taken on an SGI Origin 2000 (4×195 MHz R10000 processors, 512 Mb RAM).

Scheme	$\sigma = 10^4$, $t_{end} = 0.020$			$\sigma = 10^5$, $t_{end} = 0.005$		
	k_{max}	Vol. loss	CPU	k_{max}	Vol. loss	CPU
RK1	1.3×10^{-5}	0.028	114.31	1.0×10^{-6}	0.044	372.49
RK4	8.0×10^{-5}	0.024	66.51	3.0×10^{-5}	0.044	44.16
FE/BE	7.0×10^{-5}	0.044	28.45	1.0×10^{-5}	0.052	49.00
MP	8.0×10^{-5}	0.084	56.62	2.5×10^{-5}	0.068	44.00
	1.6×10^{-4}	0.131	29.99	5.0×10^{-5}	0.119	26.72

Moving to the *MP* scheme, we saw already in Table VI that coupling the fibre and fluid together within an iteration does allow much larger time step to be taken than for explicit schemes. However, there is a corresponding increase in the rate of volume leakage, which is given in the "Vol. loss" column in Table VII as a change in area relative to the initial 0.251 cm^2. We chose two representative time steps for the *MP* scheme in Table VII, from which it is clear that while stability restrictions are much more lenient than for the other schemes, the method suffers from a much more severe loss of volume if k is taken too large. In fact, there is no advantage to using the iterative scheme if we require a comparable level of volume loss to that experienced by the other schemes.

We can conclude from these results that while the *MP* iteration may be unconditionally convergent and allow significantly larger time steps to be taken, the time step is still limited by the accumulation of error in the incompressibility condition. Clearly, there is a need for more work to be done on developing new time–stepping strategies to treat the force implicitly in some type of iteration, while at the same time controlling the volume error.

Our observation that an appropriately-chosen explicit discretisation performs as well or better than any of the implicit methods used in practice (particularly when the fibre force is large) should prove to be very helpful in improving the performance of the immersed boundary method. Since the *FE/BE* method handles the fibre terms in the equations with a Forward Euler step, it seems reasonable to suppose that we can take advantage of the particular nature of the fibre modes by combining a Runge Kutta discretisation for the fibre along with implicit handling of the remaining terms in the equations. A class of schemes that fits these requirements exactly is the Implicit-Explicit Runge-Kutta (or *IMEX-RK*) family introduced in [1]. These methods have the additional advantage that they require minimal changes to the existing logic in the immersed boundary code. We applied several *IMEX-RK* methods of various orders to the immersed fibre problem, and found that the performance was comparable to the *RK4* and *FE/BE* results, with the latter differing from the first order *FE* or *RK1* method only in its implicit treatment of diffusion. While this outcome is somewhat disappointing, our straightforward implementation clearly leaves room for further investigation. We expect that more sophisticated approaches may lead to significant improvements, which may become more evident in Navier-Stokes computations with high Reynolds number, convection-dominated flows.

5 Summary and conclusions

The main questions we attempted to answer in this paper are:

1. *Why does the immersed boundary method suffer severe time-step limitations?*
2. *How does the choice of explicit or semi-implicit time discretisation influence the efficiency of the numerical scheme?*

The first question was answered by our linear analysis of the equations of motion for the immersed fibre problem with a smoothed delta-function force. The presence of an elastic fibre immersed in the flow gives rise to solution modes which, for typical parameter values, are very large in comparison to modes of Stokes' equations without an immersed fibre. In particular, these modes have large imaginary part, which points to highly oscillatory solutions. A parameter study shows that the stiffness of these fibre modes increases in severity as the viscosity is decreased and the fibre forcing is increased. Hence the limitation on time step is something quite distinct from the usual CFL limit encountered in fluid flow computations.

Before attacking the second question, we attemped to make predictions about the behaviour of explicit and semi-implicit schemes based on our analytical technique for the continuous problem. Explicit discretisations were easily evaluated by plotting the fibre modes along with the region of absolute stability for the corresponding time-stepping scheme. The clustering of the linearised fibre modes near the imaginary axis suggests that Runge-Kutta schemes (in particular, the *RK4* method) should exhibit the best performance, a hypothesis which is confirmed in numerical experiments.

Our observation that the stiffness in the problem arises from the presence of an immersed fibre in the flow suggests that an implicit discretisation should be used for the fibre terms appearing the equations. However,

previous work [26] has shown that a fully implicit scheme is extremely expensive, even for a linear forcing function. We believe that a fully coupled implicit solver might some day be developed for the more general non-linear force problem, but it seems much more reasonable to expect improvements in efficiency to come first from an application of semi-implicit methods, which couple the fluid and fibre in some form of iteration.

Keeping this in mind, we next extended our analysis to handle several semi-implicit time-stepping schemes, with an aim to developing a tool for evaluating their effectiveness, based again on the behaviour of the stiffest fibre modes. The first method we considered was the standard *FE/BE* scheme, which is the one used most often in practice. The modal analysis was used to derive time step restrictions which compared quite well with those observed in computations. The second scheme is an iterative approach proposed in [13]. We verify that the scheme is unconditionally convergent and derived convergence rates which match the behaviour of the iterations observed in numerical simulations.

The nature of the stiffness in the underlying problem suggests that considerable advantage might be gained by developing new time-stepping techniques that take into account the special characteristics of the fibre modes. While the limitation of the immersed boundary method to first order spatial accuracy is also an area of concern, the stiffness issue is of much greater import. Based on our success of our analytical approach in capturing the behaviour of the fibre modes and measuring the performance of explicit and semi-implicit discretisations, we hope that our insights can be used to develop more efficient time-stepping schemes. The particular aspects of the problem that we hope to exploit in our search are:

- the decoupling between normal and tangential fibre modes, and the fact that the stiffest modes arise from the class of tangential fibre oscillations. It is possible that some type of preconditioning strategy based on this special property of the solution, perhaps by performing a local linearisation that decouples the normal and tangential motions of the fibre, may lead to more efficient iterative schemes. A similar technique was used in [9] for removing the stiffness in interfacial flows governed by surface tension effects.

- the tendency of the fibre modes to cluster near the imaginary axis suggests that combining a Runge-Kutta discretisation of the fibre with an implicit solve for the fluid offers promise. We briefly discussed a straightforward approach based on a class of implicit-explicit Runge-Kutta schemes (given in [1]) which gave no improvement. However, we still believe that it is possible to extend the IMEX-RK framework to come up with a more efficient implementation.

Central to our investigation has been the concept of an "idealised discretisation," in which the wavenumbers are restricted to a fixed range $[1, N]$, representing the modes that can be resolved on an $N \times N$ computational grid, and by spreading the singular force over the corresponding smoothing radius $\epsilon = \frac{2}{N}$. We have therefore avoided much of the difficulty inherent in a fully discrete analysis of the problem. Nevertheless, spatially discrete effects are significant, and so we also plan to extend our analysis to this area in the future.

6 Acknowledgements

The work of J. M. Stockie was supported in part by a Post Graduate Scholarship from the Natural Sciences and Engineering Research Council of Canada (while at the University of British Columbia) and a Postdoctoral Fellowship from the Pacific Institute for the Mathematical Sciences. The work of B. R. Wetton was supported by an NSERC Research Grant. The authors would like to thank Dr. Michael Monagan, whose helpful suggestions allowed us to eke out the MAPLE determinant calculations in Section 4.

References

[1] U. M. Ascher, S. J. Ruuth, and R. J. Spiteri. Implicit–explicit Runge–Kutta methods for time–dependent partial differential equations. *Applied Numerical Mathematics, Special Issue on Innovative Time Integrators*, 25(2/3):151–168, 1997.

[2] R. P. Beyer and R. J. LeVeque. Analysis of a one-dimensional model for the immersed boundary method. *SIAM Journal on Numerical Analysis*, 29(2):332–364, 1992.

[3] Y. C. Chang, T. Y. Hou, B. Merriman, and S. Osher. A level set formulation of Eulerian interface capturing methods for incompressible fluid flows. *Journal of Computational Physics*, 124:449–464, 1996.

[4] B. W. Char et al. *Maple V Language Reference Manual*. Springer-Verlag, 1991.

[5] R. Cortez and D. A. Varela. The dynamics of an elastic membrane using the impulse method. *Journal of Computational Physics*, 138:224–247, 1997.

[6] L. J. Fauci and C. S. Peskin. A computational model of aquatic animal locomotion. *Journal of Computational Physics*, 77:85–108, 1988.

[7] A. L. Fogelson. Continuum models of platelet aggregation: Formulation and mechanical properties. *SIAM Journal on Applied Mathematics*, 52(4):1089–1110, 1992.

[8] A. L. Fogelson and C. S. Peskin. A fast numerical method for solving the three-dimensional Stokes' equations in the presence of suspended particles. *Journal of Computational Physics*, 79:50–69, 1988.

[9] T. Y. Hou, J. S. Lowengrub, and M. J. Shelley. Removing the stiffness from interfacial flows with surface tension. *Journal of Computational Physics*, 114:312–338, 1994.

[10] G. Lapenta, F. Iinoya, and J. U. Brackbill. Particle-in-cell simulation of glow discharges in complex geometries. *IEEE Transactions on Plasma Science*, 23(4):769–779, 1995.

[11] R. J. LeVeque and Z. Li. Immersed interface methods for Stokes flow with elastic boundaries or surface tension. *SIAM Journal on Scientific Computing*, 18(3):709–735, 1997.

[12] R. J. LeVeque, C. S. Peskin, and P. D. Lax. Solution of a two-dimensional cochlea model with fluid viscosity. *SIAM Journal on Applied Mathematics*, 48(1):191–213, 1988.

[13] A. A. Mayo and C. S. Peskin. An implicit numerical method for fluid dynamics problems with immersed elastic boundaries. In A. Y. Cheer and C. P. van Dam, editors, *Fluid Dynamics in Biology: Proceedings of the AMS–IMS–SIAM Joint Summer Research Conference on Biofluiddynamics (Contemporary Mathematics, vol. 141)*, pages 261–277. American Mathematical Society, 1993.

[14] M. F. McCracken and C. S. Peskin. A vortex method for blood flow through heart valves. *Journal of Computational Physics*, 35:183–205, 1980.

[15] D. M. McQueen and C. S. Peskin. Shared-memory parallel vector implementation of the immersed boundary method for the computation of blood flow in the beating mammalian heart. *Journal of Supercomputing*, 11:213–236, 1997.

[16] C. S. Peskin. Numerical analysis of blood flow in the heart. *Journal of Computational Physics*, 25:220–252, 1977.

[17] C. S. Peskin and D. M. McQueen. A three-dimensional computational model for blood flow in the heart. I. Immersed elastic fibers in a viscous incompressible fluid. *Journal of Computational Physics*, 81:372–405, 1989.

[18] C. S. Peskin and D. M. McQueen. A general method for the computer simulation of biological systems interacting with fluids. In C. P. Ellington and T. J. Pedley, editors, *Biological Fluid Dynamics*, volume 49 of *Symposia of the Society for Experimental Biology*, pages 265–276, Leeds, England, 1995.

[19] C. S. Peskin and B. F. Printz. Improved volume conservation in the computation of flows with immersed elastic boundaries. *Journal of Computational Physics*, 105:33–46, 1993.

[20] A. M. Roma. *A Multilevel Self Adaptive Version of the Immersed Boundary Method.* PhD thesis, New York University, 1996.

[21] M. E. Rosar. *A three dimensional model for fluid flow through a collapsible tube.* PhD thesis, New York University, 1994.

[22] J. M. Stockie. *Analysis and Computation of Immersed Boundaries, with Application to Pulp Fibres.* PhD thesis, Institute of Applied Mathematics, University of British Columbia, Vancouver, BC, Canada, 1997. Available at `http://www.iam.ubc.ca/theses/stockie/stockie.html` (unpublished).

[23] J. M. Stockie and S. I. Green. Simulating the motion of pulp fibres using the immersed boundary method. Submitted to *J. Comput. Phys.* Available at `http://www.math.sfu.ca/~jms/`., Nov. 1997.

[24] J. M. Stockie and B. T. R. Wetton. Stability analysis for the immersed fiber problem. *SIAM Journal on Applied Mathematics*, 55(6):1577–1591, 1995.

[25] A.-K. Tornberg, R. W. Metcalfe, L. R. Scott, and B. Bagheri. A front-tracking method for simulating fluid particle motion using high-order finite element methods. In *Proceedings of the 1997 ASME Fluids Engineering Division Summer Meeting*, Vancouver, Canada, June 22-26, 1997.

[26] C. Tu and C. S. Peskin. Stability and instability in the computation of flows with moving immersed boundaries: A comparison of three methods. *SIAM Journal on Scientific and Statistical Computing*, 13(6):1361–1376, 1992.

[27] S. O. Unverdi and G. Tryggvason. A front-tracking method for viscous, incompressible, multi-fluid flows. *Journal of Computational Physics*, 100:25–37, 1992.